Communications in Physics, Vol. 32, No. 2 (2022), pp. 169-177
DOI: https://doi.org/10.15625/0868-3166/16788

A RECTANGLE-QUARTET METAMATERIAL FOR DUAL-BAND PERFECT ABSORPTION IN THE VISIBLE REGION

NGUYEN VAN NGOC[1], NGUYEN THI HIEN[3,†], DUONG THI HA[1,4], BUI SON TUNG[1,2], BUI XUAN SON HAI[1], VU DINH LAM[1,‡], AND BUI XUAN KHUYEN[1,2,⋆]

[1]*Graduate University of Science and Technology, Vietnam Academy of Science and Technology, 18 Hoang Quoc Viet, Cau Giay, Hanoi, Vietnam*

[2]*Institute of Materials Science, Vietnam Academy of Science and Technology, 18 Hoang Quoc Viet, Cau Giay, Hanoi, Vietnam*

[3]*Faculty of Physics and Technology, TNU- University of Sciences, Tan Thinh ward, Thai Nguyen city, Thai Nguyen province, Vietnam*

[4]*Department of Physics, Thai Nguyen University of Education, Thai Nguyen, Vietnam*

E-mail: ⋆khuyenbx@ims.vast.ac.vn; †hiennt@tnus.edu.vn; ‡lamvd@gust-edu.vast.vn

Received 21 August 2021; *Accepted for publication 11 November 2021*
Published 18 March 2022

Abstract. *Based on rectangle-shaped structures, we create a dual-band metamaterial perfect absorber (DMPA) in the optical region. The independent-polarization absorption is a significant advantage as well as the simple integrated progress for constituent materials. In particular, absorption can be obtained to be over 90% in a bandwidth of 140 THz (from 608 THz to 748 THz), which is still remained well in the oblique incident angles for the TE-polarization. Our results can be regarded as the groundwork for the near future, applications such as photodetectors, energy converters, sensitive inspection technologies, and more.*

Keywords: metamaterials; perfect absorption; dual-band; visible region.

Classification numbers: 81.05.Xj; 78.67.Pt.

I. INTRODUCTION

A metamaterial perfect absorber (MPA), first devised by Landy *et al.* [1], has been spread to be the commercial uses for advanced science and technology. Since then, a near-unity absorption feature is expected to integrate into the negative-refractive index, light bender, light trapper, and reverse-Cherenkov radiator [2]. Basically, the controllable electromagnetic response is ruled by artificial resonant structures, which induce plasmonic effects from metallic and dielectric parts.

©2022 Vietnam Academy of Science and Technology

Interestingly, the magnitude and frequency of MPAs can be effectively controlled by engineering their sub-wavelength resonators [3]. Therefore, MPAs are promising resolution s for facilitating more applications, such as emitters [4–6], plasmonic sensors [7], spatial-light modulators [8], SERS [9], food safety and so on [10].

An important future application is creating of a new generation for visible MPAs because of the standard requirements in modern optical devices integrated with them [11, 12]. Although some approaches for fabricating the single/multi-/broad-band MPAs have proven effective, for example, four-fold rotation symmetries including split-ring, square-ring, L-shaped, cross-shaped structures [13–18], and even like disk-shaped resonators and their analog forms [19–26]. However, these methods require expensive and long-term fabrication processes like the e-beam-lithography and the modern lift-off processes because of complicated structures.

In this work, we propose a simple MPA using rectangle-pair structures to achieve dual-band perfect absorption (DMPA) in a frequency range of 400-800 THz. We numerically investigate the performance of this DMPA in two special conditions: large incident angles and different polarizations of the incoming light. The dependence of absorption feature on geometrical parameters is also computed and optimized to be suitable for future fabrication such as the etching in the oxygen plasma [27, 28].

II. SIMULATION

Using the CST software, the unit cell of the proposed DMPA was designed with three sandwiched layers (metallic patterns for impedance matching- a dielectric layer - continuous metallic film), as shown in Fig. 1(a). The dielectric layer is chosen as the silicon dioxide in optical (with $\mu = 1$), which is optimized by the thickness of $t_d = 25$ nm. The thicknesses for both metallic layers (which are selected as gold with an electric conductivity of 4.56×107 S/m) are optimized to be $t_m = 6$ nm. The geometrical parameters were set to be $a = 300$, $l = 150$ and $w = 50$ nm. During the simulation, the periodic boundary conditions are applied to all unit cells in the x-y plane and open in the z-direction. The absorption $A(\omega)$ of DMPA is calculated through $A(\omega) = 1 - R(\omega) - T(\omega) = 1 - |S_{11}|^2 - |S_{21}|^2$, where $R(\omega) = |S_{11}|^2$ and $T(\omega) = |S_{21}|^2$ are the simulated reflection and transmission, respectively. Due to the thick continuous metallic plate, the light cannot penetrate through the DMPA $[T(\omega) = |S_21|^2 = 0]$, therefore, the absorption can be expressed by $A(\omega) = 1 - |S_{11}|^2$.

Based on simulated induced-charge distribution, an equivalent-circuit model can be built to describe the absorption frequencies of metamaterials [29–33]. For DMPAs, these charge currents are induced between the top and metallic bottom plates, as illustrated in Fig. 2(a) and 2(b). By initial polarization of light, an antiparallel arrangement for flowing induced charges yields a Lorentz-like magnetic response or the magnetic resonance is activated nearby perfect absorption frequency. It can be noted that, to approximately estimate the absorption frequency, the total effective values of the inductance (L_{eff}) and the capacitance (C_{eff}) in the equivalent circuit can be regarded as a function of structural parameters with negligible mutual couplings between adjacent unit cells. Consequently, the absorption frequency can be determined by $f = 1/(2\pi\sqrt{L_{eff}C_{eff}})$. It can be noted that from this Eq., the magnetic frequency of DMPAs is strongly affected by effective areas of each rectangle-shape and its arrangement along the E-field. However, the peak position depends less on the unit-cell size a and the thickness of the metallic-layer t_m [31, 32].

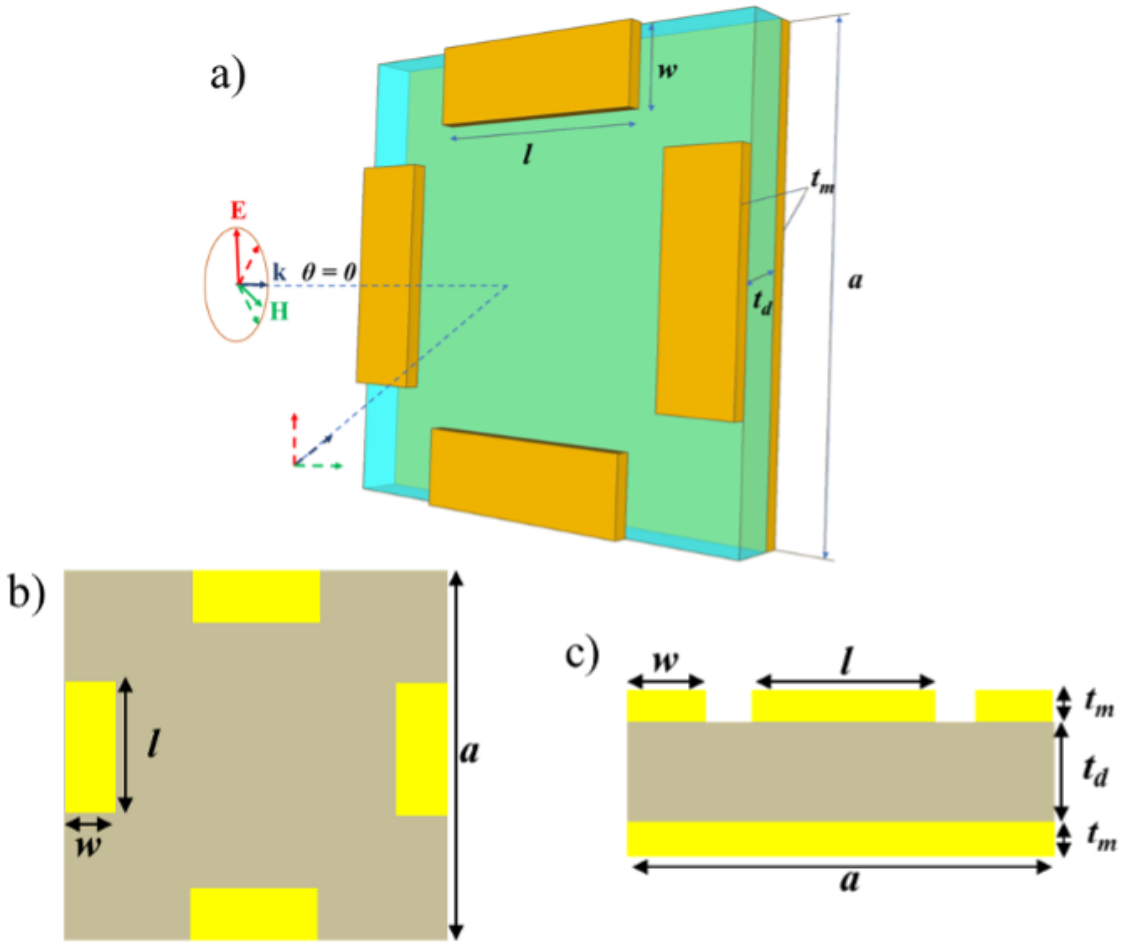

Fig. 1. (a) Three-dimensional view of a unit cell for proposed structure and its side views in (b) (E, H) and (c) (k, E) planes. Geometrical parameters are $a = 300$, $l = 150$, $w = 50$, $t_d = 25$, and $t_m = 6$ nm.

III. RESULTS AND DISCUSSION

Figures 2(a) and 2(b) show simulated absorption of single-peak MPA using only two rectangles structures, which are placed in E- and H-axial symmetry at normal incidence, respectively. Basically, in E-axial symmetry state, the single-absorption peak reaches 99.6% at 540 THz and 99.8% at 726.3 THz corresponding to polarization angles of 0 and 900 [as shown in Fig. 2(a)]. Similarly, the absorption is obtained to be 99.8% at 726.3 THz and 99.6% at 540 THz, for H-axial-symmetry case.

To clarify the original mechanism of single MPA, the parallel induced-current at these absorption peaks is presented in the inset of Figs. 2(a) and 2(b). In other words, these magnetic resonances might be a consequence of strong coupling between anti-parallel charges to an incident time-varying magnetic field (Lorentz-like magnetic response). In Fig. 2(c), we further investigate

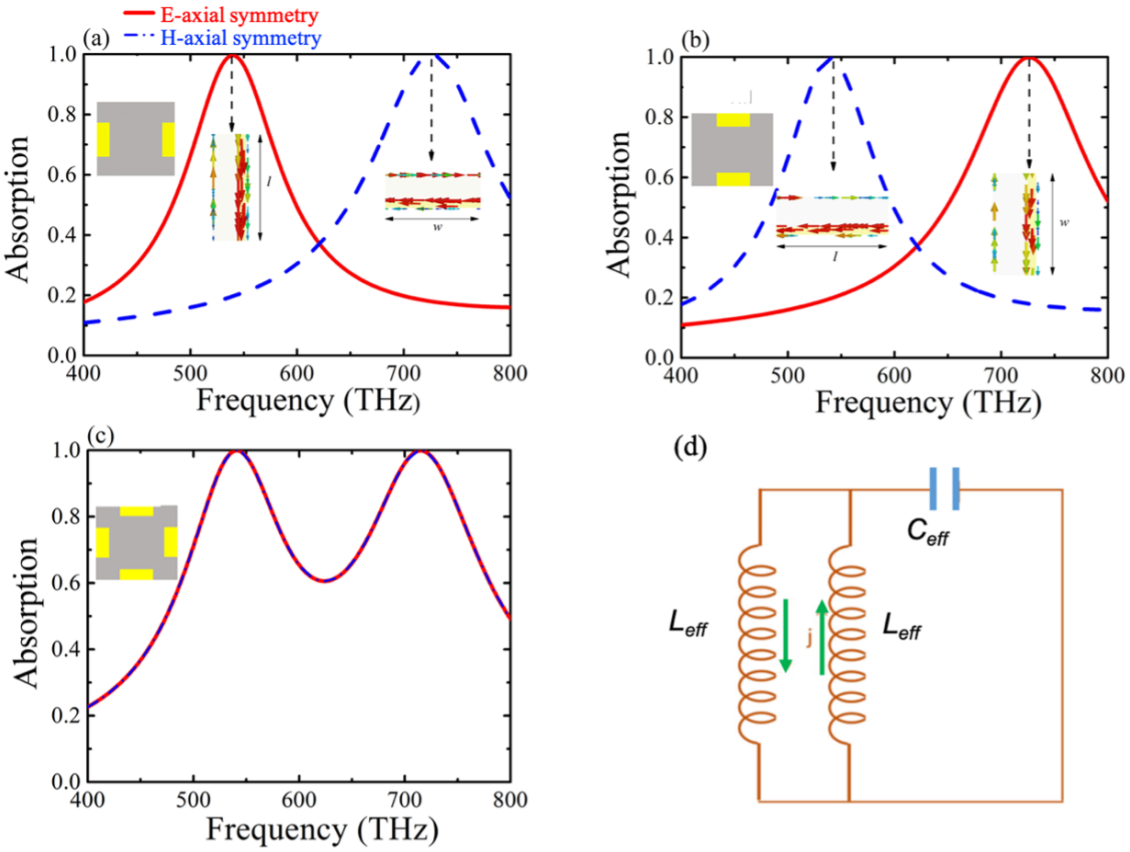

Fig. 2. Absorption spectrum of two-rectangles (a) longitudinal and (b) horizontal structures and (c) four-rectangle structures. (d) Equivalent-circuit model for single-peak MPA and/or DMPA.

how magnetic response changes in case of combining a pair of single MPA to be rectangle-quartet MPA (named as DMPA). As shown in the inset of Fig. 2(c), two perfect absorption peaks are conserved at 540.3 and 715.4 THz.

In comparison with LC-circuit model, from Fig. 2(d),the effective inductance and capacitance (for E-axial symmetry case at normal incidence) can be estimated as $L_{eff} = (t_s + 2t_m)\frac{\mu l}{4w}$(nH) and $C_{eff} = \varepsilon_0\varepsilon\gamma\frac{lw}{t_d}$(pF), where ε, μ and γ are the permittivity of the SiO_2 layer, the permeability of the dielectric spacer and the geometrical factor (which is exploited for precise effective-capacitance area), respectively. In this case, the calculated absorption frequencies are approximately valued as $f_E = 539.5$ THz (with $\gamma = 0.24$). For H-axial symmetry case at normal incidence, the absorption frequency can be determined by $f_H = 727.1$ THz (with $\gamma = 0.44$, $L_{eff} = (t_s + 2t_m)\frac{\mu w}{l}$ and $C_{eff} = \varepsilon_0\varepsilon\gamma\frac{lw}{t_d}$). The different values of geometrical factor γ in the effective capacitance due to the induced charges are accumulated at a specific area on the top and bottom metallic layer (at different magnetic resonances) [34–36]. These calculated results are agreed well with the simulated ones.

To get more insight into the absorption mechanism of DMPA, the distributions for induced magnetic energy at resonant frequencies are investigated, as shown in Fig. 3. It can be seen that the induced magnetic energy is strongly enhanced at locations of bottom-up and left-right rectangles at 540.3 and 715.4 THz, respectively. This observation confirms the magnetic nature of the dual-absorption peak, which is caused by anti-parallel currents on the meta-surface and its mirror [31, 32]. In particular, these localized distributions support the aforementioned assumption that the mutual coupling between two single-peak MPA in the super cell are small and can be ignored in the calculation.

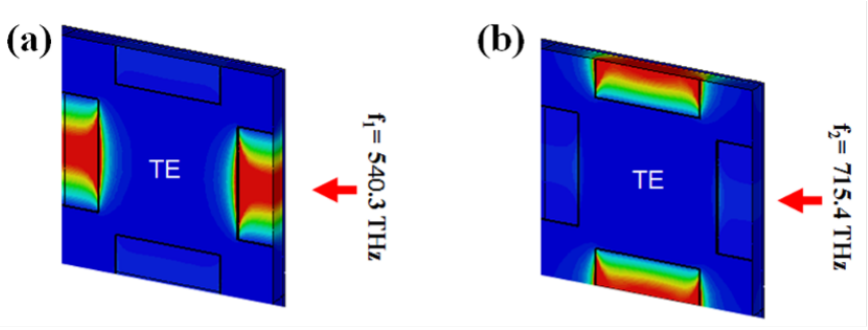

Fig. 3. Induced magnetic-energy distributions at (a) 540.3 THz and (b) 715.4 THz at normal incidence.

In order to emphasize the advantages of DMPA, the impact of periodicity a on the absorption spectra are investigated and shown in Fig. 4. The trend of simulated absorption spectra is observed with various a from 0.2 to 0.5 μm while other parameters are fixed in Fig. 4(a). The simulated absorption intensity declines considerably from 100% to 62% without shifting the absorption peak since a is changed from 0.3 to 0.5 μm. It can be noted that the optimized lattice constant is $a = 0.3$ μm, where the near-unity absorption can be created by a good matching condition between DMPA and the surrounding environment. It should be noted that when the lattice constant is 0.2 μm, the impedance mismatching can be occurred due to the reduction in amplitude (resonant strength) of effective permeability and/or permittivity. Similarly, in Fig. 4(b), when the dielectric thickness td increases from 0.02 μm to 0.035 μm (for $a = 0.3$ μm), the absorption is reduced to below 90%. As shown in Fig. 4(c), the absorption spectrum of the proposed structure is almost unaffected by the metal layer thickness.

From equations estimated for f_E and f_H, the absorption frequencies are strongly influenced by the width and the length of the rectangle-quartet shape due to the large changes of Leff and C_{eff}. In detail, Fig. 4(d) plots the dependence of absorption spectrum (absorption over 98%) on the l, which is increased slightly from 0.1 to 0.175 μm ($w = 0.050$ μm). The first absorption peak f_E is gradually shifted towards the higher frequency (from 610.4 to 745.6 THz) and the second absorption peak fH is almost unchanged. In contrast, in Fig. 4(e), since the width w is grown from 0.03 to 0.06 μm, the fH tends to be gradually shifted to a lower frequency while the fE is maintained. These results can be explained by changing the cross-section of the resonators in the direction of the applied magnetic field corresponding to the enhancement or reduction of the effective inductance and capacitance, consequently, the absorption frequencies tend to be decreased or increased.

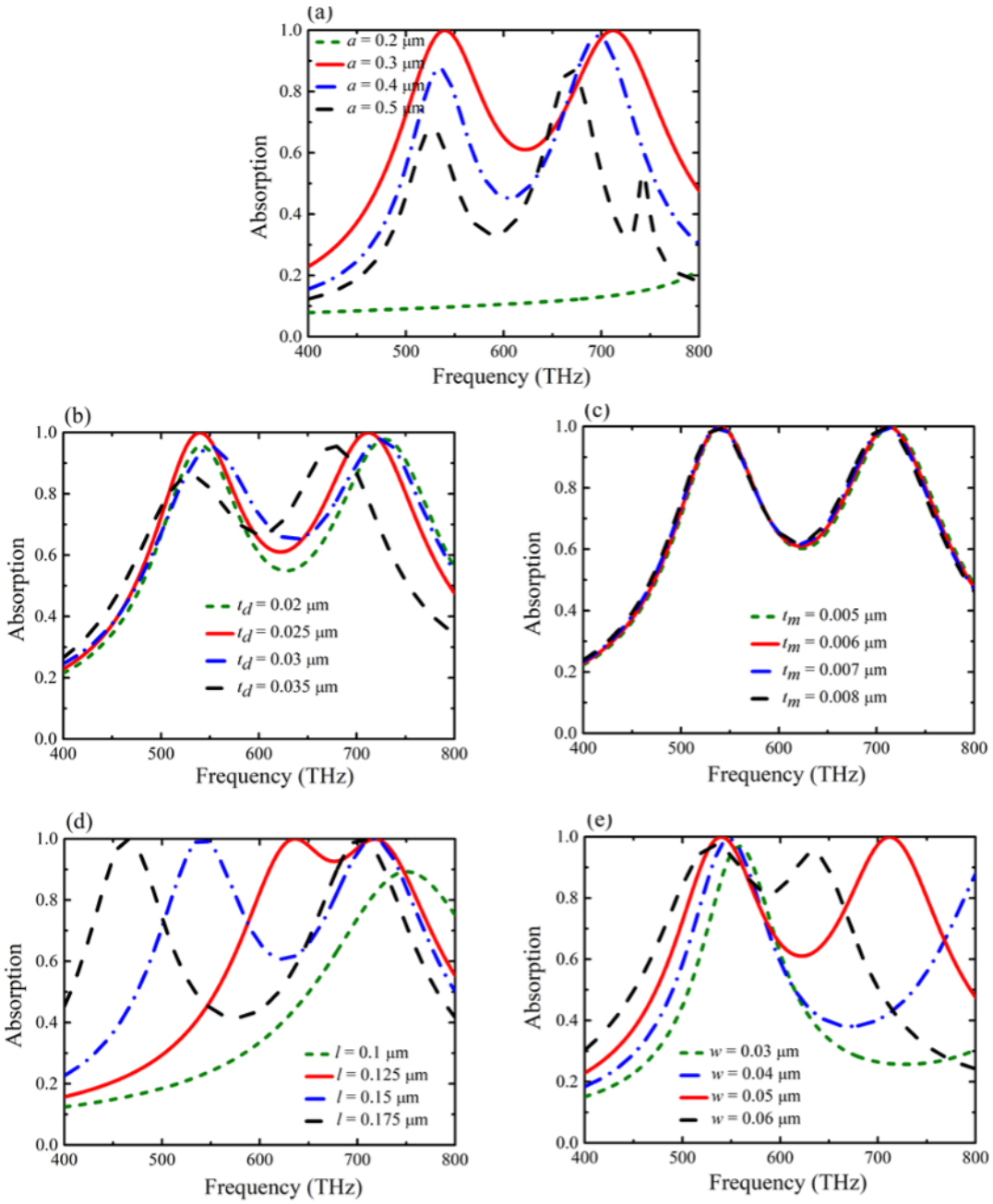

Fig. 4. The dependence of the absorption spectrum on (a) the lattice constant a; (b) the dielectric thickness td, (c) thickness of the metal layer tm, (d) length l, and (e) width w of the rectangle.

In general, the future integrated applications require DMPAs that need to be wide-incident-angle and polarization-insensitive performance. Therefore, the dependence of absorption spectra

on transverse electric (TE) mode and different polarized angles of the incoming light is simulated in Fig. 5. The proposed DMPA is basically constructed from the symmetric arrangement of rectangle shapes and it is clearly independent with every polarization angle (for normal incidence) as shown in Fig. 5(a). For TE-mode, the simulated dual-band absorption is maintained to be above 95% since the incident angle is smaller 30˚. For larger angles, the absorption starts decreases considerably due to the impedance mismatching (by the strength downgrade of the excited H-field projected on the sample plane at a large incident angle). As shown in Fig. 5(b), for incident angle tends to be 45˚, the absorptions are detected to be 100% at 681.6 THz and 89% at 607.2 THz. The perfect-absorption behavior at fH can be explained by a more comprehensive absorption mechanism, where the high loss caused by the magnetic resonance might be not the only single consumption.

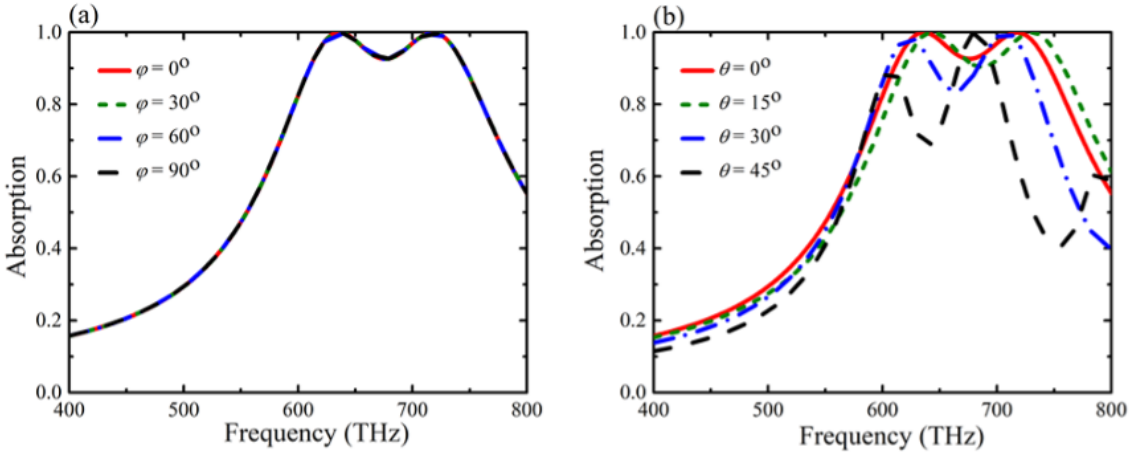

Fig. 5. Simulated absorption spectra working with different (a) polarization angles (b) incident angles.

IV. CONCLUSIONS

We designed, simulated, and numerically characterized the dual-band perfect absorption with the polarization-insensitive and wide-angle performance of MM in the optical region. The proposed DMPA is simple and suitable for future fabrication techniques such as the etching in the oxygen plasma and more. To predict and control the operating frequencies, the equivalent circuit model is examined and shown an outstanding agreement to the simulated results. Our work demonstrated that the absorption features would be useful for a comprehensive understanding of the absorption mechanism for next generations of metamaterials, which are relevant to realize commercial applications like photodetectors, energy converters, etc.

ACKNOWLEDGMENT

This research is funded by Graduate University of Science and Technology under Grant Number GUST.STS.ĐT2019-KHVL01, and by Vietnam National Foundation for Science and Technology Development (NAFOSTED) grant number 103.99-2020.23.

REFERENCES

[1] N. I. Landy, S. Sajuyigbe, J. J. Mock, D. R. Smith and W. J. Padilla, *Perfect metamaterial absorber*, *Phys. Rev. Lett.* **100** (2008) 207402.

[2] Y. Liu and X. Zhang, *Metamaterials: a new frontier of science and technology*, *Chem. Soc. Rev.* **40** (2011) 2494.

[3] N. I. Zheludev and Y. S. Kivshar, *From metamaterials to metadevices*, *Nat. Mater.* **11** (2012) 917.

[4] X. Liu, T. Tyler, T. Starr, A. F. Starr, N. M. Jokerst and W. J. Padilla, *Taming the blackbody with infrared metamaterials as selective thermal emitters*, *Phys. Rev. Lett.* **107** (2011) 045901.

[5] C.-M. Wang, Y.-C. Chang, M. N. Abbas, M.-H. Shih and D. P. Tsai, *T-shaped plasmonic array as a narrow-band thermal emitter or biosensor*, *Opt. Express* **17** (2009) 13526.

[6] J. J. Lai, H. F. Liang, Z. L. Peng, X. Yi and X. F. Zhai, *MEMS integrated narrow band infrared emitter and detector for infrared gas sensor*, *Journal of Physics: Conference Series* **276** (2011) 012129.

[7] Q. Li, L. Cong, R. Singh, N. Xu, W. Cao, X. Zhang et al., *Monolayer graphene sensing enabled by the strong fano-resonant metasurface*, *Nanoscale* **8** (2016) 17278.

[8] W. L. Chan, H.-T. Chen, A. J. Taylor, I. Brener, M. J. Cich and D. M. Mittleman, *A spatial light modulator for terahertz beams*, *Applied Physics Letters* **94** (2009) 213511 [https://doi.org/10.1063/1.3147221].

[9] T. V. Nguyen, L. T. Pham, B. X. Khuyen, D. C. Duong, L. H. T. Nghiem, N. T. Nguyen et al., *Effects of metallic underlayer on SERS performance of a metal film over nanosphere metasurface*, *Journal of Physics D: Applied Physics* **55** (2021) 025101.

[10] Y. Zhong, L. Du, Q. Liu, L. Zhu and B. Zhang, *Metasurface-enhanced atr sensor for aqueous solution in the terahertz range*, *Opt. Commun.* **465** (2020) 125508.

[11] H.-F. Zhang, H.-B. Liu, C.-X. Hu and Z.-L. Wang, *A metamaterial absorber operating in the visible light band based on a cascade structure*, *Plasmonics* **15** (2020) 1755.

[12] W. Wang, Y. Qu, K. Du, S. Bai, J. Tian, M. Pan et al., *Broadband optical absorption based on single-sized metal-dielectric-metal plasmonic nanostructures with high-ε" metals*, *Appl. Phys. Lett.* **110** (2017) 101101.

[13] B.-X. Wang, X. Zhai, G.-Z. Wang, W.-Q. Huang and L.-L. Wang, *Frequency tunable metamaterial absorber at deep-subwavelength scale*, *Opt. Mater. Express* **5** (2015) 227.

[14] L. Huang, D. R. Chowdhury, S. Ramani, M. T. Reiten, S.-N. Luo, A. K. Azad et al., *Impact of resonator geometry and its coupling with ground plane on ultrathin metamaterial perfect absorbers*, *Appl.Phys. Lett.* **101** (2012) 101102.

[15] W. Li, X. Zhou, Y. Ying, X. Qiao, F. Qin, Q. Li et al., *Polarization-insensitive wide-angle multiband metamaterial absorber with a double-layer modified electric ring resonator array*, *AIP Adv.* **5** (2015) 067151.

[16] Y. Bai, L. Zhao, D. Ju, Y. Jiang and L. Liu, *Wide-angle, polarization-independent and dual-band infrared perfect absorber based on l-shaped metamaterial*, *Opt. Express* **23** (2015) 8670.

[17] L. Huang and H.-T. Chen, *A brief review on terahertz metamaterial perfect absorbers*, *Terahertz Sci. Technol.* **6** (2013) 26.

[18] P. Pitchappa, C. P. Ho, P. Kropelnicki, N. Singh, D.-L. Kwong and C. Lee, *Dual band complementary metamaterial absorber in near infrared region*, *Journal of Applied Physics* **115** (2014) 193109.

[19] C. M. Watts, X. Liu and W. J. Padilla, *Metamaterial electromagnetic wave absorbers*, *Advanced Materials* **24** (2012) OP98 [https://onlinelibrary.wiley.com/doi/pdf/10.1002/adma.201200674].

[20] C.-Y. Tsai, S.-P. Lu, J.-W. Lin and P.-T. Lee, *High sensitivity plasmonic index sensor using slablike gold nanoring arrays*, *Applied physics letters* **98** (2011) 153108.

[21] C.-W. Cheng, M. N. Abbas, C.-W. Chiu, K.-T. Lai, M.-H. Shih and Y.-C. Chang, *Wide-angle polarization independent infrared broadband absorbers based on metallic multi-sized disk arrays*, *Opt. Express* **20** (2012) 10376.

[22] D. Viet, N. Hien, P. Tuong, N. Minh, P. Trang, L. Le et al., *Perfect absorber metamaterials: Peak, multi-peak and broadband absorption*, *Optics Communications* **322** (2014) 209.

[23] S. Guddala, R. Kumar and S. A. Ramakrishna, *Thermally induced nonlinear optical absorption in metamaterial perfect absorbers*, *Appl. Phys. Lett.* **106** (2015) 111901 [https://doi.org/10.1063/1.4914451].

[24] A. D. Khan, M. Amin, A. Ali, S. D. Khan and R. Khan, *Multiple higher-order fano resonances in plasmonic hollow cylindrical nanodimer*, *Appl. Phys. A* **120** (2015) 641.
[25] Q. Wang, W. Han, P. Liu and L. Dong, *Electrically tunable quasi-3-d mushroom plasmonic crystal*, *J. Lightwave Technol.* **34** (2016) 2175.
[26] P. Jahangiri, F. B. Zarrabi, M. Naser- Moghadasi, A. Saee Arezoomand and S. Heydari, *Hollow plasmonic high q-factor absorber for bio-sensing in mid-infrared application*, *Optics Communications* **394** (2017) 80.
[27] J. Kaschke and M. Wegener, *Optical and infrared helical metamaterials*, *Nanophotonics* **5** (2016) 510.
[28] G. M. Crouch, C. Oh, K. Fu and P. W. Bohn, *Tunable optical metamaterial-based sensors enabled by closed bipolar electrochemistry*, *Analyst* **144** (2019) 6240.
[29] L. N. Le, N. M. Thang, L. M. Thuy and N. T. Tung, *Hybrid semiconductor–dielectric metamaterial modulation for switchable bi-directional thz absorbers*, *Optics Communications* **383** (2017) 244.
[30] D. T. Viet, N. V. Hieu, V. D. Lam and N. T. Tung, *Isotropic metamaterial absorber using cut-wire-pair structures*, *Appl. Phys. Express* **8** (2015) 032001.
[31] J. Zhou, E. N. Economon, T. Koschny and C. M. Soukoulis, *Unifying approach to left-handed material design*, *Opt. Lett.* **31** (2006) 3620.
[32] N. T. Tung, D. T. Viet, B. S. Tung, N. V. Hieu, P. Lievens and V. D. Lam, *Broadband negative permeability by hybridized cut-wire pair metamaterials*, *Appl. Phys. Express* **5** (2012) 112001.
[33] N. T. Tung and T. Tanaka, *Characterizations of an infrared polarization-insensitive metamaterial perfect absorber and its potential in sensing applications*, *Photonics Nanostructures: Fundam. Appl.* **28** (2018) 100.
[34] N. T. Hien, L. N. Le, P. T. Trang, B. S. Tung, N. D. Viet, P. T. Duyen et al., *Characterizations of a thermo-tunable broadband fishnet metamaterial at thz frequencies*, *Comput. Mater. Sci.* **103** (2015) 189.
[35] T. Q. H. Nguyen, T. K. T. Nguyen, T. N. Cao, H. Nguyen and L. G. Bach, *Numerical study of a broadband metamaterial absorber using a single split circle ring and lumped resistors for x-band applications*, *AIP Adv.* **10** (2020) 035326 [https://doi.org/10.1063/1.5143915].
[36] T. H. Nguyen, T. A. H. Nguyen, T. N. Dinh, X. K. Bui, S. T. Bui, X. C. Nguyen et al., *Multiband metamaterial absorber in a ring structure base on high-order magnetic resonance*, *Comm. in Phys.* **31** (2021) 199.